ACCEPTED MANUSCRIPT
Review of Scientific Instruments
AIP Publishing
This is the author's peer reviewed, accepted manuscript. However, the online version of record will be different from this version once it has been copyedited and typeset.
PLEASE CITE THIS ARTICLE AS DOI:10.1063/5.0012404

Intrinsic thermal interfacial resistance measurement in bonded metal-polymer foils

Manjunath C. Rajagopal[1*], Timothy Man[1], Adreet Agrawal[1], Gowtham Kuntumalla[1], and Sanjiv Sinha[1].

[1]*Department of Mechanical Science and Engineering, University of Illinois at Urbana-Champaign, Urbana, IL 61801, USA.*

Abstract

Heat conduction through bonded metal-polymer interfaces often limits the overall heat transfer in electronics packaging, batteries, and heat recovery systems. To design the thermal circuit in such systems, it is essential to measure the thermal interfacial resistance (TIR) across ~1-100 μm junctions. Previously reported TIR of metal-polymer junctions utilize ASTM E1530-based two-block systems that measure the TIR by applying pressure across the interface through external heating and cooling blocks. Here, we report a novel modification of the ASTM-E1530 technique that employs integrated heaters and sensors to provide an intrinsic TIR measurement of an adhesively bonded metal-polymer junction. We design the measurement technique using finite element simulations to either passively suppress or actively compensate the lateral heat diffusion through the polymer, which can minimize the systematic error to $\lesssim 5\%$. Through proof-of-concept experiments, we report the TIR of metal-polymer interfaces made from DuPont's Pyralux double-side copper-clad laminates, commonly used in flexible printed circuit boards. Our TIR measurement errors are $<10\%$. We highlight additional sources of errors due to non-idealities in the experiment and discuss possible ways to overcome them. Our measurement technique is also applicable to interfaces that are electrically insulating such as adhesively-joined metal-metal junctions and sputter-coated or welded metal-polymer junctions. Overall, the technique is capable of measuring TIR $\gtrsim 10^{-5}$ m^2 KW^{-1} in bonded metal-polymer foils, and can be tailored for *in situ* measurements in flexible electronics, circuit packaging, and other hybrid metal-polymer systems.

I. Introduction

Bonded metal-polymer interfaces are used in devices ranging from wearable electronics [1], [2] batteries [3], [4] and heat recovery systems [5]–[7] to avionics [8], [9]. Accurate measurement

*email: chinnap2@illinois.edu

Review of Scientific Instruments
ACCEPTED MANUSCRIPT
AIP Publishing
This is the author's peer reviewed, accepted manuscript. However, the online version of record will be different from this version once it has been copyedited and typeset.
PLEASE CITE THIS ARTICLE AS DOI:10.1063/5.0012404

of their intrinsic thermal interfacial resistance (TIR) can inform the design of thermal systems [10], help in assessing joining methods [11], and provide an additional means of evaluating the interface *in situ* [3], [12]. For instance, the heat flux across batteries [3], [13], thermoelectric coolers [14], [15] and heat spreaders [16], [17] in electronics packaging are often limited by the thermal resistance of their interfaces, which are ~10^{-5}-10^{-3} $m^2 KW^{-1}$. Similarly, in composite heat recovery systems, the effective thermal conductivity and the profitability of heat recovery is dependent on the thermal interfacial resistance [6], in particular on metal-polymer TIR in the range 10^{-5}-10^{-3} $m^2 KW^{-1}$. Such metal-polymer interfaces, especially in electronics packaging [16] and batteries [3], often deteriorate over time due to cyclic loading, which increases the TIR and can even lead to thermal runaway [4], [18]. Thus, measuring the intrinsic thermal interfacial resistance *in situ* on the metal-polymer interfaces could be useful for thermal management, [15], [17], [19] and interface evaluation [3], [12].

The thermal interfacial resistance (TIR) arises from two sources. At microscopic scales, differences in vibrational and electronic states of the materials on either side of an interface scatter energy carriers such as electrons and phonons, leading to a resistance R''_{Ka}, also called Kapitza resistance [20]. The Kapitza resistance is ~10^{-9}-10^{-7} $m^2 KW^{-1}$[21], [22], and is of importance in atomically smooth interfaces typically formed in cleanroom environments under vacuum conditions. The equivalent thermal interface thickness ($L_K = k.R''$) or the Kapitza length of atomically smooth interface on dielectric substrates (k~1 $Wm^{-1}K^{-1}$) is < 0.1 μm. On the other hand, at more macroscopic scales, asperities at the interface reduce the total area of contact and create crowding of heat flow lines, leading to a second component in the TIR, R''_{asp} [8]. In a vast majority of industrial applications, the macroscopic component R''_{asp} dominates the overall thermal interfacial resistance. For interfaces with R''_{asp}~ 10^{-5}-10^{-3} $m^2 KW^{-1}$ on a polymer substrate (k~0.1 $Wm^{-1}K^{-1}$), the Kapitza length, L_K, is ~1-100 μm Consequently, the penetration depth (heat diffusion length-scale) of a TIR measurement must be in the order of L_K~100 μm or more to ensure that the measurement is sensitive to the interface.

Currently, techniques such as the 3ω-method [23]–[25], frequency domain and time domain thermo-reflectance (FDTR and TDTR) [26]–[28], [28] are used for microscopic TIR measurements (of relatively smooth junctions). For frequency-domain measurements, the

Review of Scientific Instruments ACCEPTED MANUSCRIPT
This is the author's peer reviewed, accepted manuscript. However, the online version of record will be different from this version once it has been copyedited and typeset.
PLEASE CITE THIS ARTICLE AS DOI:10.1063/5.0012404
AIP Publishing

penetration depth is given by, $d = \sqrt{\alpha/\pi f}$, where, α is the thermal diffusivity and f is the modulation frequency. In the typical frequency range of measurements ~5 Hz – 100 kHz for 3ω and ~0.3 MHz – 20 MHz for FDTR [29], the penetration depth d is <80 μm and <0.1 μm, respectively, when the substrate is a polymer (α~0.1 mm^{2}s^{-1}) [30]. Since the penetration depth d is less than the Kapitza length L_K~100 μm, frequency domain techniques such as 3ω and FDTR are not suitable for measuring such interfaces. For time-domain measurements, the penetration depth is given by, $d = \sqrt{\tau\alpha}$, where τ is the measurement timescale and α is the thermal diffusivity. TDTR typically uses femtosecond laser pulses (pump) with a probe time delay of few nanoseconds (τ~ 10 ns) [31], which has a penetration depth, d of ~30 nm in a polymer substrate. Transient thermo-reflectance (TTR) employs nanosecond lasers with up to τ~10 μs delay time [32], which has a penetration depth, d of ~1 μm in a polymer substrate. Since time-domain techniques such as TTR and TDTR have penetration depth $d \lesssim 1$ μm, they are also not suited for measuring the TIR of interfaces with a Kapitza length, L_K~100 μm. We note that the values of penetration depth and Kapitza length were estimated using α and k of substrate (polymer); however, the outcome does not change if we use copper's thermal properties. In general, the state-of-the-art TIR measurement techniques are suited for atomically smooth interfaces made in cleanroom environment and not for high TIR interfaces (10^{-5}-10^{-3} m^2 KW^{-1}) that are common in industrial applications.

Instead, TIR measurements of thick junctions ($L_K \gtrsim 100$ μm) typically resort to steady-state ASTM standards (D5470/E1530) that use two blocks at different temperatures to sandwich the sample [33]–[36]. Such measurements have been used to report the contact resistance of metal-polymer-metal [36], or metal-metal blocks kept under pressure. However, the contact resistance of two blocks under pressure is not representative of the intrinsic TIR of bonded interfaces that are welded or adhesively joined. For instance, changing the pressure applied across two contacting blocks by 0-3 MPa can change the measured TIR by an order of ~10^3 [36], [37]. On the other hand, interfaces used in electronics packaging [10], [38], [39], aviation [8] [9], and other commercial applications are often bonded using adhesives or welds. Adhesively bonded interfaces are typically cured at high temperatures and pressures (~190°C and 2 MPa) [40], which also improves the physical adsorption and diffusion between the adhesive and adherent [41]. Similarly, welding processes can locally melt the interface, reducing the grain size, and increasing the surface area of the contact [42], [43]. Such bonded interfaces may exhibit different intrinsic interfacial resistance

Review of Scientific Instruments
ACCEPTED MANUSCRIPT
AIP Publishing
This is the author's peer reviewed, accepted manuscript. However, the online version of record will be different from this version once it has been copyedited and typeset.
PLEASE CITE THIS ARTICLE AS DOI: 10.1063/5.0012404

in comparison to the previously reported TIR of two surfaces kept under pressure. In summary, existing steady-state TIR measurement techniques used for thermally thick junctions (L_T ≳100 μm) do not measure the intrinsic TIR of bonded interfaces.

In this work, we adapt techniques used previously for measuring the thermal conductivity of thin films [44] to introduce a novel modification to the ASTM-E1530 standard. The main modification is to employ an integrated heater and sensor. Here, we demonstrate the technique using proof-of-concept experiments to measure the intrinsic TIR of copper-Kapton junctions bonded using adhesives but the technique can be used on any metal-polymer junction (L_K ≫1 μm) made through techniques ranging from sputtering [45] to electroplating [46] to welding (laser [47], friction-stir [43], or ultrasonic [48]). Such metal-polymer junctions are used in emerging applications such as wearable electronics [1], [2], flexible solar cells [49], [50], Li-ion batteries [3], and hybrid heat exchangers [6]. This paper is organized as follows. Section II develops the concept of our TIR measurement technique using finite element simulations. We specifically design the measurement to minimize systematic errors to $< 5\%$. Section III describes the fabrication and the measurement process of an experiment that uses the optimized design to measure the TIR of adhesively joined copper-Kapton interface. We explain the experimental results in Section IV. Section V discusses the results, applications, and limitations of our TIR measurement technique. We also discuss additional sources of errors due to non-idealities in our experiments. Our integrated measurement technique can be suitably designed to have an error ≲10% for TIR ≳10^{-5} m^2 KW^{-1} in any metal-polymer interface as well as adhesively-bonded metal-metal interfaces.

II. Experiment Design

In this Section, we discuss experimental design aspects for measuring the intrinsic TIR of bonded metal-polymer junctions, whose Kapitza length (L_K) is ~1-100 μm. At macroscopic scales, metal-polymer TIR measurements [36], [37] were typically performed using external heating and cooling metal blocks that sandwich a polymer block under external pressure. However, such two-block systems do not measure the intrinsic TIR since the polymer is cured outside of the TIR

ACCEPTED MANUSCRIPT
Review of Scientific Instruments
AIP Publishing
This is the author's peer reviewed, accepted manuscript. However, the online version of record will be different from this version once it has been copyedited and typeset.
PLEASE CITE THIS ARTICLE AS DOI: 10.1063/5.0012404

measurement setup [36], [37]. On the other hand, at microscopic scales, spin-coated polymers and evaporated metals can be patterned into a micromesa structure [44] to measure the intrinsic metal-polymer TIR. However, the micromesa technique is limited to polymers that can be spin-coated and patterned, which is usually <5 µm thick [44]. Widely used polyimides like Kapton are chemically resistant [51], [52] to conventional patterning processes [53], [54]. To this end, we devise a technique that keeps the polymer intact, and instead patterns the metal as heaters and temperature sensors (Figure 1). A cross-section view of the TIR test section is shown in Figure 1a, and the electrical four-point probe connections to the heater and temperature sensors are shown in Figure 1b. A subtle issue in keeping the polymer intact arises from the lateral heat diffusion through the polymer that must be accounted for in the TIR measurements. We explain the experiment design process in this section for adhesively joined copper-Kapton junctions made from Dupont's double-side clad laminates [40] as a test case; however, it can also be extended to sputter-coated [45], electroplated [46], or welded [47], [48] metal-polymer junctions.

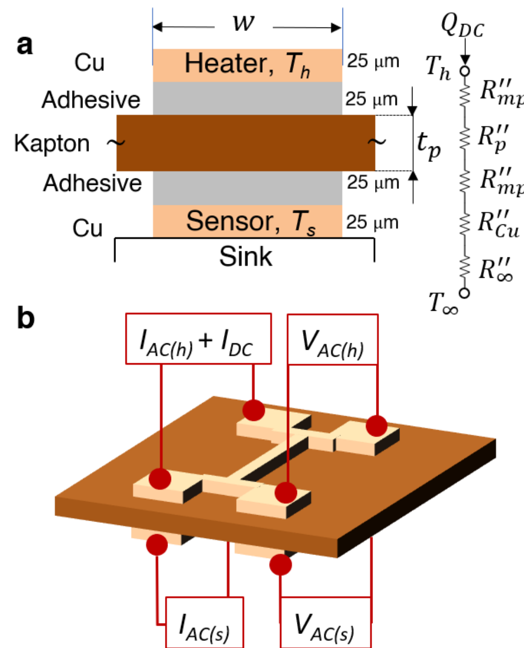

Figure 1. a) Schematic of the TIR test section, showing a cross-section. Typical values of t_p are 25-75 µm. Representative of a sample made using DuPont Pyralux copper-clad laminate. b) Schematic of the electrical connections for temperature measurement and heating.

ACCEPTED MANUSCRIPT
Review of Scientific Instruments
AIP Publishing
This is the author's peer reviewed, accepted manuscript. However, the online version of record will be different from this version once it has been copyedited and typeset.
PLEASE CITE THIS ARTICLE AS DOI:10.1063/5.0012404

The metal on either side of the laminate is patterned as four-point probes that act as heaters and temperature sensors. The sample is placed on a sink (or fixture) such that only the sensor metal film is in contact with the fixture. The contact pads on the backside (sensor) can be made accessible through the top side during fabrication. In Section III, we explain in detail one of the possible ways of implementing such a measurement setup, whereas the current section focuses on developing the concept of the measurement technique. A heat flow, Q_{DC}, can be supplied to the heater line using a DC current, I_{DC}. Both the heater and the sensing lines' temperatures (T_h and T_s) can be simultaneously measured through the four-point probe resistances. The thermal interfacial resistance between the metal and polymer (R''_{mp}) can be extracted using Eq. (1) by assuming a 1D heat conduction through the test section.

$$\frac{\Delta T_h - \Delta T_s}{Q_{DC}} = \frac{t_p}{k_p A} + \frac{2R''_{mp}}{A} \qquad (1)$$

where, t_p is the thickness of the polymer, k_p is the polymer's thermal conductivity, A is the area of the interface, and R''_{mp} is the thermal interfacial resistance of a unit area. If the polymer's thermal conductivity k_p is not known a priori, the thermal interface resistance R''_{m-p} can still be extracted (through Equation (1)) by using test sections of different polymer thickness (t_p). We separately measured Kapton's thermal conductivity to be 0.17 $Wm^{-1}K^{-1} \pm 0.01\ Wm^{-1}K^{-1}$ (see Supplementary Information, Figure 2), which is used throughout the study. We can then extract the TIR, R''_{mp}, from the slope of a linear fit to Equation (1) for different heat inputs.

The polymer laterally extends beyond the test section for structural integrity, and ease of fabrication and external connections. Lateral heat diffusion through the polymer introduces a systematic error in the TIR measured through a 1D assumption (Equation (1)). To investigate this possibility, we use finite element simulations of the measurement process in COMSOL to understand when the 1D assumption fails. Figure 1a shows the geometry of the 2D model used for the simulations. We assumed that the Kapton extends to about 5 mm on either side. We use 400 $Wm^{-1}K^{-1}$ as the thermal conductivity of copper. A heat input of Q_{DC} was given to the heater at the top. The bottom of the sensor was assumed to have a thermal resistance, R''_{∞} (~ $4\times10^{-4}\ m^2KW^{-1}$) to the sink ($T_{\infty}$), which corresponds to the sample holder's thermal resistance taken from our previous work [55]. The outcome of the simulations is insensitive to R''_{∞}, which we discuss further in Section V. We perform our measurements in a vacuum cryostat, and consequently, we applied

1 adiabatic boundary conditions elsewhere for the simulations. We initially provide a certain thermal
2 resistance, R''_{mp}, as a material property for the adhesive, and then extract the same from the
3 simulation results using Eq. (1). We denote the difference between the input TIR (R''_{mp}) and its
4 extracted value as $\Delta R''_{mp}$, which is indicative of the absolute error in the TIR measurement.

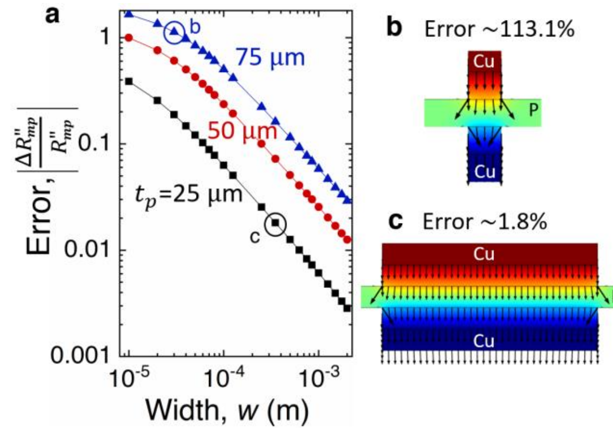

5

6 Figure 2. a) Simulated error in TIR measurements plotted as a function of test section width (w) and
7 polymer thickness (t_p). The circled points are used for the contours shown in the adjacent figures. b) Heat
8 flux lines and temperature contours for a narrow test junction (30 µm). c) Contours for a wider junction
9 (350 µm). For all the points shown here, the TIR, R''_{mp} = 10^{-4} m^2KW^{-1}

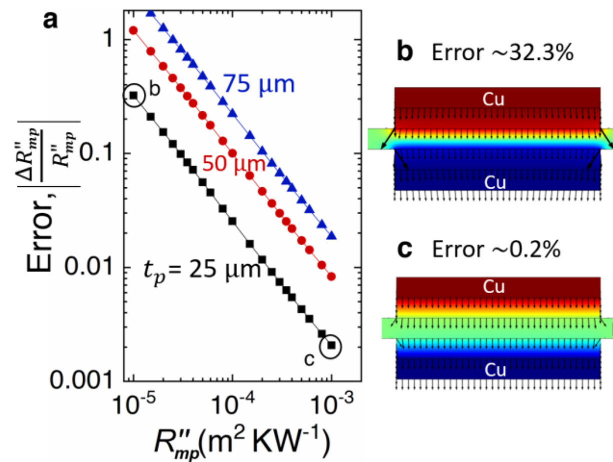

10

11 Figure 3. a) a) Simulated error in TIR measurements plotted as a function of the TIR (R''_{mp}) and polymer
12 thickness (t_p). The circled points are used for the contours shown in the adjacent figures. b) Heat flux
13 lines and temperature contours for a low TIR (10^{-5} m^2KW^{-1}) junction. c) Contours for a high TIR (10^{-3}
14 m^2KW^{-1}) junction. For all the points shown here, test section width, w = 250 µm.

Review of Scientific Instruments
ACCEPTED MANUSCRIPT
This is the author's peer reviewed, accepted manuscript. However, the online version of record will be different from this version once it has been copyedited and typeset.
PLEASE CITE THIS ARTICLE AS DOI:10.1063/5.0012404
AIP Publishing

ACCEPTED MANUSCRIPT
Review of Scientific Instruments
AIP Publishing
This is the author's peer reviewed, accepted manuscript. However, the online version of record will be different from this version once it has been copyedited and typeset.
PLEASE CITE THIS ARTICLE AS DOI:10.1063/5.0012404

1 Lateral heat diffusion through the polymer depends on the test section's width (w), polymer
2 thickness (t_p) and the TIR (R''_{mp}). We first examine the relative error, $\left|\Delta R''_{mp}/R''_{mp}\right|$, as a function of
3 the test section width, w, and the polymer thickness, t_p, in Figure 2. Irrespective of polymer
4 thickness, the error reduces with increasing width. For a wider test section, the proportion of the
5 lateral heat diffusion is smaller, as evident from the heat flux lines in Figure 2b, c. Further, thicker
6 polymer junctions require wider test sections to reduce lateral heat diffusion. For the errors to be
7 < 10%, the required width of the test section is >60 µm, 250 µm, and 625 µm for 25 µm, 50 µm,
8 and 75 µm polymer thickness, respectively. We then choose 250 µm as the test section width to
9 examine the error as a function of the TIR (R''_{mp}) and the polymer thickness (t_p) in Figure 3.
10 Notably, we find that the error decreases with increasing interfacial resistance (R''_{mp}). For a low
11 interfacial resistance (R''_{mp}~10^{-5} m^2KW^{-1}), most of the temperature drop appears across the
12 polymer, increasing the lateral heat diffusion (Figure 3b). On the other hand, at high interfacial
13 resistance (~10^{-3} m^2KW^{-1}), the temperature drops primarily across the adhesive, reducing the
14 lateral heat diffusion through polymer (Figure 3c). Overall, whenever the polymer's thermal
15 resistance dominates the overall transverse resistance of the test section, lateral heat diffusion
16 through the polymer increases.

17 For a 1D heat conduction, a wider test section is always preferable. However, from a
18 measurement perspective, a wider test section produces a smaller temperature change (ΔT_h-ΔT_s)
19 and requires more heating current (I_{DC}), as shown in Figure 4. We show the current required and
20 temperature changes across the test section for 10 mW heating power to measure TIR~ 10^{-3} -10^{-5}
21 m^2KW^{-1}. The current required, I_{DC}, is calculated from Q_{DC}=I_{DC}^2R, assuming the electrical
22 resistivity of copper ~1.7×10^{-8} Ω.m. Assuming a conservative temperature measurement error of
23 ~0.5 K, data points below the dashed line (~0.5 K) are not measurable (shaded region in Figure
24 4a). Similarly, assuming a maximum amperage for the electrical leads in the cryostat to be ~1 A,
25 the data points in the corresponding shaded region (>1 A) in Figure 4b are not suitable. The range
26 of widths, w, under the shaded region is not suitable. If we trace the x-axis of Figure 4 from left to
27 right, the highest width, w, that is not under any shaded region is the optimum width for the test
28 section. Data points leaning toward higher widths are preferred since they have low systematic
29 errors from a reduced 2D heat conduction. This figure therefore provides a guideline for choosing
30 the appropriate width for the test section, given the expected range of the thermal interfacial

ACCEPTED MANUSCRIPT
Review of Scientific Instruments
AIP Publishing
This is the author's peer reviewed, accepted manuscript. However, the online version of record will be different from this version once it has been copyedited and typeset.
PLEASE CITE THIS ARTICLE AS DOI: 10.1063/5.0012404

1 resistance. We note that Figure 4 is plotted for a heating power of 10 mW, which suggests an
2 optimal w = 250 µm. Similar analysis can be performed if higher heating power (>10 mW) can be
3 supplied through high amperage electrical leads to enable a measurable ΔT (>0.5 K) in wider test
4 sections (>250 µm). For the experiments reported in this study, we use 10 mW and hence choose
5 a width, w~250 µm to curtail systematic error to ≲10% since we expect the thermal resistance to
6 be in the range 10^{-3}-10^{-4} m^2KW^{-1}. If the expected TIR is ~10^{-5} m^2KW^{-1} (say, for the conditions in
7 Figure 3b) the systematic error can still be reduced to <10% by actively compensating for lateral
8 heat diffusion using additional heaters, which we explain later in Section V. We also discuss
9 additional sources of errors due to potential non-idealities in the experiment in Section V.

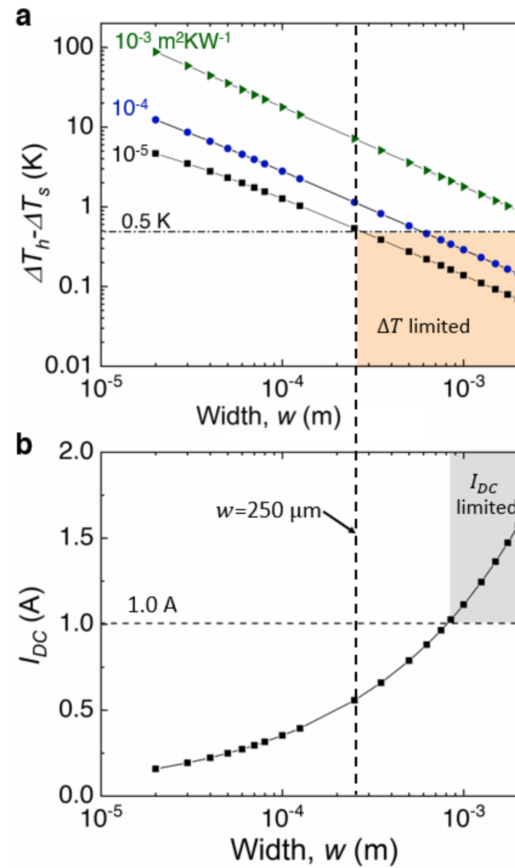

10

11 Figure 4. a) The simulated temperature difference across the test section are plotted for test sections of
12 different widths. b) The calculated DC current required is plotted for test sections of different widths.
13 Heating power of 10 mW and polymer thickness, t_p = 25 µm, are assumed for all the points shown here.
14 The shaded regions correspond to limitations in measurement either due to a low-temperature difference
15 (<0.5 K) or a high current (>1 A) requirement.

III. Fabrication and Measurements

Using simulations, we predicted that a test section width of 250 μm is appropriate for our metal-polymer junctions. In this section, we first describe the fabrication steps to pattern the test section with heaters and temperature sensors (schematically represented in Figure 1), and then we explain the measurement process. Our test samples were adhesively bonded copper-Kapton junctions made from DuPont's Pyralux LF copper-clad laminates [40]. Specifically, we used LF9111R, LF9121R, and LF9131R, which has 25 μm, 50 μm, and 75 μm thick Kapton, respectively. The Kapton was bonded to copper on either side using acrylic-based adhesives (~25 μm thick). Such laminates are commonly used in flexible printed circuit boards [40], and hybrid heat exchangers [56] owing to its high-temperature (~100°C) stability.

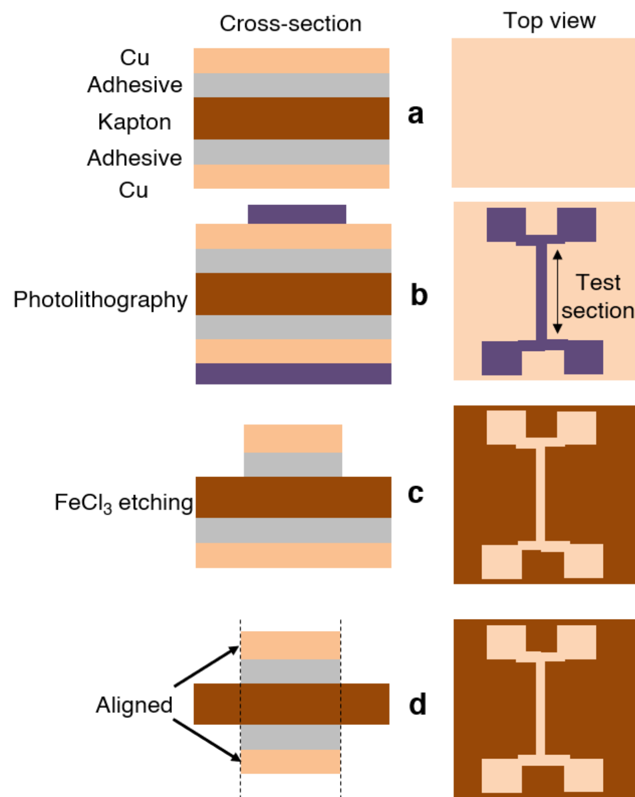

Figure 5. a) Schematic shows the composition of copper-clad laminates. b) Photoresist on top side is photolithographically patterned to resemble a four-point probe heater. c) Copper is etched using the photoresist as a mask using ferric chloride. d) The process is repeated on the backside to form a four-point probe sensor.

Review of Scientific Instruments
ACCEPTED MANUSCRIPT
This is the author's peer reviewed, accepted manuscript. However, the online version of record will be different from this version once it has been copyedited and typeset.
PLEASE CITE THIS ARTICLE AS DOI: 10.1063/5.0012404
AIP Publishing

Review of Scientific Instruments
ACCEPTED MANUSCRIPT
AIP Publishing
This is the author's peer reviewed, accepted manuscript. However, the online version of record will be different from this version once it has been copyedited and typeset.
PLEASE CITE THIS ARTICLE AS DOI:10.1063/5.0012404

We patterned heating and sensing elements with four-point-probes (4pp) on either side of the copper-clad laminates through a process depicted in Figure 5. We first spun photoresist on the backside of the laminate to protect it. The photoresist on the topside was then patterned to form the heater of the test section (250 µm wide and ~1.3 cm long), with 4-point-probe contact pads (Figure 5b). The photoresist pattern served as an etch mask to pattern the underlying copper using a ferric chloride-based copper etchant solution (from Transene Inc.), as shown in Figure 5c. The copper etching was performed at 40°C for around 15 minutes. Steps *b* and *c* of Figure 5 were repeated on the backside of the laminate to pattern the sensing line (Figure 5d). The heater and sensing lines (250 µm wide) were aligned with each other using a backside alignment photolithography step. We removed the photoresist using a typical degreasing procedure (acetone, and isopropyl alcohol). Figure 6 shows optical images and a schematic of the fabricated test samples and the sample fixture. The sensing line's 4pp contact pads (5-8) on the backside were made accessible on the frontside using silver paint (Figure 6b). To ensure that the test section's bottom copper film (sensor) is the only component attached to the sink (as shown in Figure 1a), we use a Kapton tape with a small window (~3 mm) of adhesive exposed on the chip holder (Figure 6a). The test sample is then placed by orienting the test section along the exposed adhesive (Figure 6c). The test section was gently pressed using a wire bonder capillary to ensure that the bottom copper film (sensor) is firmly in contact with the exposed adhesive (Figure 6d). We note that this technique may result in additional heat pathways through the extended polymer that could be in contact with the sample fixture (sink). We discuss the possible errors due to the additional heat pathways in Section V. The samples were wire bonded to the exposed contact pads 1-8 on the front side (Figure 6c).

ACCEPTED MANUSCRIPT
Review of Scientific Instruments
AIP Publishing
This is the author's peer reviewed, accepted manuscript. However, the online version of record will be different from this version once it has been copyedited and typeset.
PLEASE CITE THIS ARTICLE AS DOI:10.1063/5.0012404

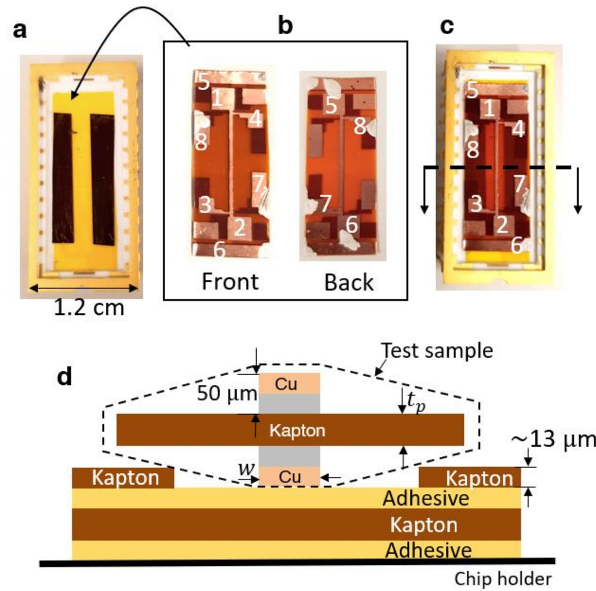

Figure 6. Optical image and schematic of sample fixture. a) An optical image of the sample holder that has a Kapton base with exposed adhesive. b) Optical images of a representative test sample shown with numbered contact pads. Silver paste was used to bring the back-side connections to the front. c) The test sample is placed on the sample holder and the test section is attached to the exposed Kapton adhesive. A cross-section of the image in c) is shown in a schematic in d). d) A Kapton tape with double-side adhesive is first attached to the chip holder. A thin (~13 µm) Kapton tape is used to limit the exposed adhesive to the vicinity of test section.

The interfacial resistance measurement is a two-step process. In the first step, the temperature coefficient of electrical resistance (TCR) of the heating and sensing line is measured individually by measuring changes in the electrical resistance at different bath temperatures of the cryostat. The bath temperature of the cryostat can be controlled with an accuracy of 1 mK. We used Keithley 6221 as an AC current source for both heater ($I_{AC(h)}$) and sensor ($I_{AC(s)}$) lines (Figure 1b). Two lock-in amplifiers (SR830) were used for voltage measurements across the heater ($V_{AC(h)}$) and sensor ($V_{AC(s)}$). Using the calibrated TCRs, we then estimate the temperature changes at the heater and sensor. In the second step, we used a Keithley source meter to send DC current (I_{DC}) ranging from 0 to 0.6 A in steps of 0.1 A to the heating line. The corresponding temperature changes at the heater (ΔT_h) and sensor (ΔT_s) lines can be used to extract the thermal interfacial resistance of the

ACCEPTED MANUSCRIPT
Review of Scientific Instruments
This is the author's peer reviewed, accepted manuscript. However, the online version of record will be different from this version once it has been copyedited and typeset.
PLEASE CITE THIS ARTICLE AS DOI:10.1063/5.0012404
AIP Publishing

metal-polymer junction (R''_{m-p}) using equation (1). The overall error in measuring the interfacial thermal resistance of the metal-polymer junction is:

$$\delta(R''_{m-p}) = \frac{A}{2}\sqrt{\left(\delta\left(\frac{(\Delta T_h - \Delta T_s)}{Q_{DC}}\right)\right)^2 + \left(\frac{t_p}{k_p^2 A}\delta(k_p)\right)^2} \tag{2}$$

The error in measuring the temperature difference is given by $\delta(\Delta T_i) = -\Delta T_i \times \delta(TCR_i)/TCR_i$, where TCR is the temperature coefficient of resistance, $i = h$(heater) or s(sensor). The error component $\delta(TCR)$ corresponds to the 95% confidence interval of the slope of resistance change, dR/R, vs, temperature, T. Similarly, the first term in Eqn. (2) corresponds to the 95% confidence interval for the slope of (ΔT_h-ΔT_s) vs Q_{DC}. The error in measuring the polymer's thermal conductivity, $\delta(k_p)$ is explained in the supplementary information.

IV. Results

We first measured the temperature coefficient of electrical resistance (TCR) of the heater and sensing line. For a test sample using t_p=50 µm, we measured the TCR of the heater and sensing line at 300 K to be 2.38 × 10^{-3} K^{-1} $\pm$1.02% and 2.48 × 10^{-3} K^{-1} $\pm$0.83%, respectively. The measured TCRs are lower than the bulk value ~4 × 10^{-3} K^{-1} [57], possibly due to stressvoiding [58] in copper, induced during adhesion process or fabrication, which may also be amplified by being on a flexible substrate. We then provided a DC current to the heater ranging from 0 to 0.6 A. The corresponding temperature changes at heater and sensor are plotted in Figure 7. Even though the heater's temperature rises to ~15 K above 300 K at I_{DC}=0.6 A, the overall temperature difference between the heater and sensor is only ~3.1 K. The solid lines represent the corresponding results from the simulation. We fit the simulation to experimental data using R''_{∞} as a fitting parameter, since it can change with experimental conditions. From the figure, the experimental data seems to closely follow the predicted trends from the simulation.

ACCEPTED MANUSCRIPT
Review of Scientific Instruments
AIP Publishing
This is the author's peer reviewed, accepted manuscript. However, the online version of record will be different from this version once it has been copyedited and typeset.
PLEASE CITE THIS ARTICLE AS DOI:10.1063/5.0012404

1 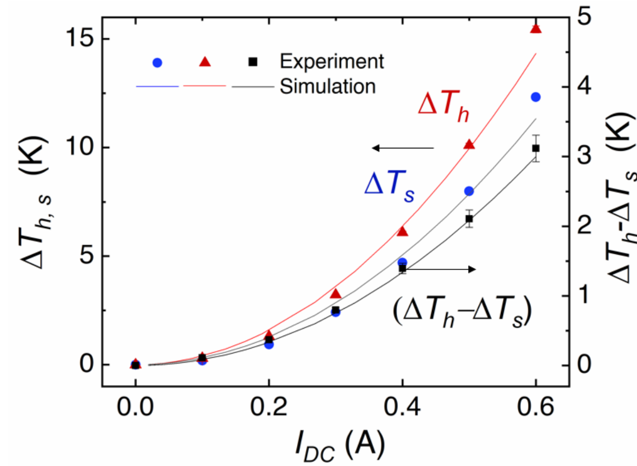

2 Figure 7. Temperature changes at heater (in red triangles) and sensor (in blue circles) are plotted along the
3 left y-axis for different heating currents. The overall temperature difference between heating and sensing
4 lines (black squares) is plotted along the right y-axis. The solid lines represent the corresponding
5 simulation results with R''_∞~3.4 × 10^{-3} m^2 KW^{-1}. The error bars correspond to 1σ measurement errors.
6 This graph corresponds to a sample with t_p=50 µm and is representative of all samples used in this study.

7

8 The interfacial thermal resistance between metal and polymer (R''_{m-p}) can be extracted
9 from the slope of a linear fit shown as a dashed line in Figure 8, using Eq. (1). We separately
10 measured Kapton's thermal conductivity to be 0.17 $Wm^{-1}K^{-1}$ $\pm$ 0.01 $Wm^{-1}K^{-1}$ (Supplementary
11 Figure 2). Using the appropriate thickness (t_p) and thermal conductivity (k_p), the interfacial
12 thermal resistance (R''_{m-p}) for a sample with t_p=50 µm was found to be 3.1 × 10^{-4} m^2 KW^{-1}. We
13 calculate the measurement error from Eq. (2) to be $\pm$3.5%. From simulations, we predict the
14 systematic error to be 2.9%. Together, the total error is $\pm$4.6%. We repeated the measurements on
15 other test samples with t_p=25 µm and 75 µm. The average thermal interfacial resistance (R''_{m-p})
16 of all the measured copper-Kapton junctions were 3.7× 10^{-4} m^2 KW^{-1}, with a measurement error
17 of $\pm$4.1%. The corresponding systematic errors estimated from simulations were 0.8%, and 5.7%,
18 for the test samples with 25 µm, and 75 µm thick Kapton. The overall error is ~$\pm$4.7%, dominated
19 by measurement errors.

ACCEPTED MANUSCRIPT
Review of Scientific Instruments
AIP Publishing
This is the author's peer reviewed, accepted manuscript. However, the online version of record will be different from this version once it has been copyedited and typeset.
PLEASE CITE THIS ARTICLE AS DOI:10.1063/5.0012404

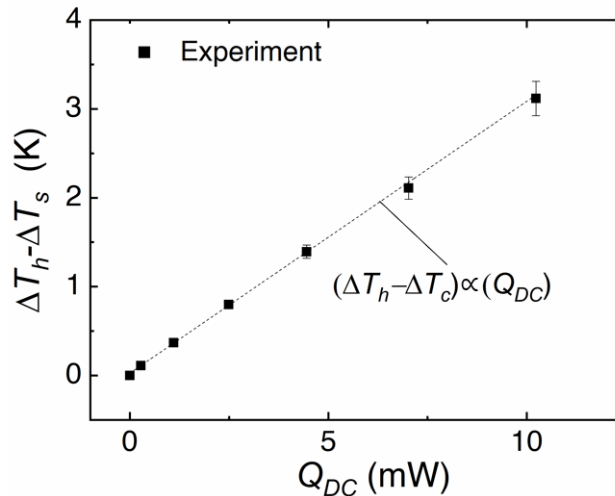

Figure 8. The temperature difference between the heater and the sensor line is plotted against the input heating power. The dashed line represents a linear fit to the data. The error bars correspond to 1σ measurement errors. This graph corresponds to a sample made with t_p=50 μm and is representative of all samples used in this study

V. Discussion

In this work, we designed the TIR measurement technique using simulations and experimentally implemented the measurement on a copper-Kapton junction. Below, we analyze the results of our measurements, additional sources of errors, and then discuss the applications and limitations of the measurement technique.

We used finite element simulations to predict the error in TIR measurements. For the simulations in Section II, we used an estimate for R''_∞ (~ 4×10^{-4} m^2KW^{-1}) that is different from the extracted value (~3.4×10^{-3} m^2 KW^{-1}) using experimental data in Figure 7. However, this does not change the predicted systematic error in TIR measurements. The value of R''_∞ only affects ΔT_h and ΔT_s, but does not influence the overall temperature difference (ΔT_h-ΔT_s), since it appears outside the resistance network used for Equation (1). Further, we were limited to 250 μm wide test sections, since our rated amperage was 1 A for the electrical leads in the cryostat (Figure 4). Future work can utilize higher heating power (>10 mW) on wider test sections (>1 mm) using high amperage (>1 A) or multi-strand electrical leads to reduce the systematic errors. A wider test section can also reduce fabrication complexity. The results on experimental design presented in Section II provide a general framework for designing measurements and they can be customized

to suit different experimental conditions such as the available heating power, test section dimensions, and the expected measurement errors.

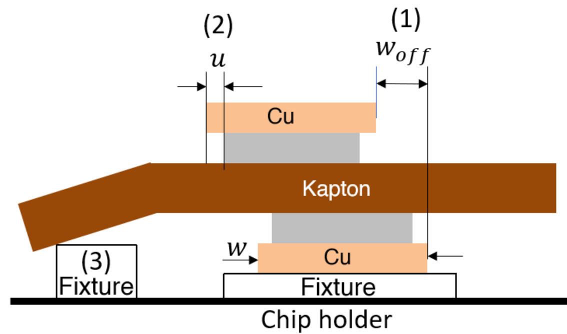

Figure 9. Schematic of non-idealities in the experimental measurement of the thermal interface resistance. (1) represents offset error due to misalignment. (2) represents undercut of the adhesive during fabrication. (3) represents additional heat pathways due to the extended polymer.

In Section II, we developed the concept of our measurement technique. However, experimental implementation of the measurement could result in non-idealities that could introduce additional sources of error. In Figure 9, we show three primary sources of error: (1) offset (w_{off}) between the heater and sensor due to misalignment, (2) undercut (u) of the adhesive during fabrication, (3) additional heat pathways through the extended polymer that could be in contact with the sample fixture materials. The error in TIR measurement increases with the misalignment (w_{off}), reaching up to ~10% for w_{off}=50 µm if the test section width is 250 µm (Supplementary Figure 3b). The misalignment error becomes less significant if the test section is wider. For instance, for a test section of 1 mm width, a higher misalignment w_{off}= 100 µm results in a TIR error of ~10%. For our samples, the misalignment (w_{off}) is typically less than 25 µm, and hence the corresponding contribution to the overall error is negligible (<5%). An undercut, u, could locally crowd the heat flux lines, which could result in a 2D heat spreading across the test section. Assuming a typical undercut, u ~ 25 µm, corresponding to the thickness of the adhesive, we use computations to find that the error in TIR could increase from 2.9% (without undercut) to 6.9% (with undercut) for a sample with t_p=50 µm, and width w=250 µm. The error in TIR due to undercut could also be reduced by using a wider test section. For instance, for a test section of w=1 mm, the error in TIR could be 1.5% with an undercut of 25 µm. During fabrication, undercut could be reduced by using anisotropic RIE etching using O_2 to remove the photoresist instead of acetone. The TIR

Review of Scientific Instruments
ACCEPTED MANUSCRIPT
AIP Publishing
This is the author's peer reviewed, accepted manuscript. However, the online version of record will be different from this version once it has been copyedited and typeset.
PLEASE CITE THIS ARTICLE AS DOI:10.1063/5.0012404

Review of Scientific Instruments
ACCEPTED MANUSCRIPT
AIP Publishing
This is the author's peer reviewed, accepted manuscript. However, the online version of record will be different from this version once it has been copyedited and typeset.
PLEASE CITE THIS ARTICLE AS DOI:10.1063/5.0012404

measurement error due to additional heat pathways from the extended polymer is difficult to predict computationally since the contact resistances of additional pathways between the polymer and the fixture are unknown. We instead performed experiments using thermal paste to fix the test section to the chip holder (Supplementary Figure 4). Since the spreading of thermal paste is difficult to control, it creates additional pathways for the heat to flow from polymer to the chip holder directly. We repeated our TIR measurements on the same samples to find that the average TIR is 3.4×10^{-4} $m^2 KW^{-1} \pm 8.4\%$ when thermal paste was used. When the samples were fixed with thermal paste, the TIR is roughly 10% smaller than the average TIR reported in Section IV, possibly due to additional heat pathways. However, since the difference is comparable to the error in the measurements, we believe that the additional heat pathways either did not contribute to any significant error in TIR, or our measurement is insensitive to the difference. Further, we measured the Kapton's thermal conductivity separately through ASTM E1530 standard, by stacking multiple Kapton layers together (supplementary information). The measured thermal conductivity was 0.17 $Wm^{-1}K^{-1}$ for Kapton HN films, which is within the range (0.12-0.23 $Wm^{-1}K^{-1}$) of previously reported values for Kapton [52], [59]. However, since we assumed the interfacial resistance between Kapton layers to be negligible, the measured thermal conductivity of Kapton, k_p, is representative of a lower bound. Our TIR measurement is therefore representative of a lower bound and serves as a proof-of-concept experiment to demonstrate our TIR measurement technique on adhesively joined metal-polymer interface. Future work can measure Kapton's thermal conductivity separately by using 3ω or TDTR via thin metal films evaporated directly on Kapton, or use test sections of different t_p to extract the TIR (R''_{mp}) (Eqn. (1)).

The systematic error in TIR measurements can be further reduced by using additional heaters to actively compensate for the lateral diffusion of heat through polymer. By supplying an additional heat, say Q_{ref}, from either side of the test section, we could compensate for the portion of heat from Q_{DC} that diffused laterally through the polymer. Figure 10b shows a schematic of the additional heaters that can supply a heat Q_{ref}, whose temperature T_{ref} can also be measured using four-point probes. The optimum Q_{ref} can be found experimentally, by monitoring the temperature,

$$\Delta T_{comp} = \left|\frac{\Delta T_{ref} + \Delta T_s}{2}\right|_{Q_{DC}=0} - \left|\frac{\Delta T_{ref} + \Delta T_s}{2}\right|_{Q_{ref}=0} \qquad (3)$$

Review of Scientific Instruments ACCEPTED MANUSCRIPT
This is the author's peer reviewed, accepted manuscript. However, the online version of record will be different from this version once it has been copyedited and typeset.
PLEASE CITE THIS ARTICLE AS DOI:10.1063/5.0012404
AIP Publishing

which goes to zero for a certain Q_{ref} that compensates the lateral heat diffusion. The first component of ΔT_{comp} in Eqn. (3) is representative of the temperature change in Kapton near the test section, due to the additional heat (Q_{ref}) in the absence of heating at test section (Q_{DC}). The second component corresponds to the average temperature at the Kapton near the test section due to the heat, Q_{DC}. By balancing these two components we can roughly compensate for the lateral heat diffusion. We explore this aspect using finite element simulations for two test cases shown in Figure 10a. For a test section with 25 μm thick Kapton and TIR=10^{-5} m^2KW^{-1}, we could reduce the TIR measurement error from ~32.3% (Figure 3b) to ~0.2% (Figure 10c) by providing a heat Q_{ref}=0.08Q_{DC} (red points in Figure 10a). Similarly, for a test section with 100 μm thick Kapton and TIR = 10^{-4} m^2KW^{-1}, the error in TIR measurements can be reduced from ~38.9% to ~2.0% by using Q_{ref}=0.23Q_{DC} (black points in Figure 10a). This compensation technique can be readily implemented experimentally to find and supply Q_{ref}, and it requires fabricating two additional four-point probes. The compensation technique cannot reduce the thermal gradients everywhere in the polymer film. It reduces the lateral temperature gradient in the polymer film at close proximity to the test section, as evident from Supplementary Figure 5. We note that the definition of ΔT_{comp} may not apply to all cases, especially if t_p >100 μm and TIR<10^{-5} m^2KW^{-1}, where the temperature drop across Kapton is large and requires an explicit temperature measurement of Kapton near the test section for compensation. In such cases, numerical simulations can be used to find the optimum Q_{ref}. Further, an estimation of the additional heat required, Q_{ref}, is also limited by the error in measuring ΔT_{comp}. In general, the active compensation technique utilizing additional heaters can reduce the systematic errors in the range of ~20-50% (without compensation) to ≲10% (with compensation), which can be useful in cases where t_p > 50 μm and TIR<10^{-4} m^2KW^{-1} (Figure 3).

ACCEPTED MANUSCRIPT
Review of Scientific Instruments
AIP Publishing
This is the author's peer reviewed, accepted manuscript. However, the online version of record will be different from this version once it has been copyedited and typeset.
PLEASE CITE THIS ARTICLE AS DOI:10.1063/5.0012404

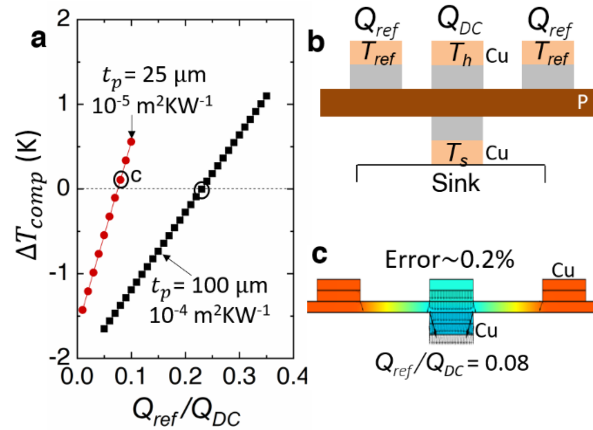

Figure 10 a) Compensation heat (Q_{ref}) is varied to find out the optimum at which the lateral heat diffusion is compensated, which occurs at $\Delta T_{comp} \sim 0$. The results shown here are obtained from simulations. Q_{DC} =10 mW, w = 250 µm. b) A schematic of the additional heaters that are placed adjacent to the test section. c) Temperature contours are shown along with the heat flux lines for the chosen Q_{ref} from a). This figure is drawn to scale, with the width of the test section w=250 µm.

The design of our experiment enables *in situ* and intrinsic TIR measurement, and its related applications. Since our technique leaves the polymer layer intact, it allows for a TIR evaluation that can be readily integrated into existing flexible electronics and circuit packaging. In-situ thermal interface resistance measurement can then be used to evaluate the degree of delamination of the interface [12]. Especially, flexible and wearable electronic circuits are often subjected to cyclic loading, which can delaminate the metal leads from the polymer, substrates [60], increasing the TIR. Similarly, thermal interfacial material (TIM) [16] in chip packaging, and electrode-separator interfaces [3] in Li-ion batteries can deteriorate over time, which increases their TIR and under extreme conditions results in a thermal runaway [4], [18]. By suitably tailoring our measurement design, an *in situ* TIR measurement can help to evaluate the interface delamination.

Although we report measurements on adhesively-joined copper-Kapton junctions in this study, this TIR measurement technique is generally applicable to any metal-polymer junction and even certain metal-metal junctions. Such metal-polymer junctions made using sputtering [45], adhesives [40], mechanical fastening [61], or welding [47], [48], find applications in automotive sector [47], [62], flexible electronics [1], [40], and hybrid thermal management devices [6], [63]. Moreover, this TIR measurement technique can be used on metal-metal junctions that are adhesively bonded

ACCEPTED MANUSCRIPT
Review of Scientific Instruments
AIP Publishing
This is the author's peer reviewed, accepted manuscript. However, the online version of record will be different from this version once it has been copyedited and typeset.
PLEASE CITE THIS ARTICLE AS DOI:10.1063/5.0012404

together, which are used in hybrid heat exchangers [6], [56], and in aircraft industries [64], where high strength-to-weight ratio joints are preferred.

Our TIR measurement technique requires the junction to have metal surfaces on either side that can be patterned as a heater and a sensor. The integrated sensors also require the junction to be electrically insulating in the cross-plane direction, which is available in most printed circuit boards and other electronics packaging. Typical candidates could be metal-polymer-metal junctions, or metal-metal junctions joined using adhesives or TIM that are electrically insulating. For such metal-polymer-metal junctions, a deterministic TIR measurement is possible if the polymer's thermal conductivity is known a priori, or it can be statistically extracted using test sections of different polymer thickness t_p. Overall, our TIR measurement technique applies to any combination of materials at the junction as long as the interface is electrically insulating.

VI. Conclusion

In summary, we report an integrated sensing technique to measure the intrinsic thermal interfacial resistance (TIR) of bonded interfaces. On a metal-polymer interface, we microfabricated heaters and temperature sensors using the metal layer, which were calibrated *in situ* for the TIR measurement. We kept the polymer layer intact to minimize fabrication complexity and potentially enable *in situ* applications. To reduce the lateral heat diffusion through the polymer, we use finite element simulations to design the test section and curtail systematic errors to $<5\%$. Through proof-of-concept experiments, we measured the metal-polymer TIR to be ~3.7 × 10^{-4} m^2 KW^{-1} $\pm$ 4.7% for DuPont Pyralux copper-Kapton laminates that were adhesively bonded. This technique is extendable to sputter-coated, electroplated, or welded metal-polymer interfaces as well as adhesively-bonded metal-metal interfaces with TIR $\gtrsim 10^{-5}$ m^2 KW^{-1}. For TIR measurements on junctions with thick polymers (>50 μm) or low TIR ($<10^{-4}$ m^2 KW^{-1}), we developed an active compensation technique utilizing additional heaters to further reduce the systematic error in TIR measurements to $<10\%$. We also discussed additional sources of errors due to non-idealities in the experiments and provided ways to overcome them. Our TIR measurement technique requires the polymer's thermal conductivity to be known, or it can be extracted by using test sections of different polymer thicknesses. Our measurement framework can be suitably adapted for *in situ* TIR measurements in flexible electronics, batteries, or chip packaging to evaluate an interface.

ACCEPTED MANUSCRIPT
Review of Scientific Instruments
AIP Publishing
This is the author's peer reviewed, accepted manuscript. However, the online version of record will be different from this version once it has been copyedited and typeset.
PLEASE CITE THIS ARTICLE AS DOI:10.1063/5.0012404

Supplementary Material

See supplementary material for a description of Kapton's thermal conductivity measurement using a technique similar to ASTM E1530 standard.

Acknowledgments

We acknowledge support from the Advanced Manufacturing Office (AMO) of the Office of Energy Efficiency and Renewable Energy (EERE) under the U.S. Department of Energy, through the contract DE-EE0008312. This work was partly carried out in Holonyak Micro-Nano Technology Laboratory (HMNTL) and Frederick Seitz Materials Research Laboratory (FS-MRL) at the University of Illinois, Urbana, IL.

Data Availability

The data that support the findings of this study are available from the corresponding author upon reasonable request.

References

[1] M. Virili, H. Rogier, F. Alimenti, P. Mezzanotte, and L. Roselli, "Wearable Textile Antenna Magnetically Coupled to Flexible Active Electronic Circuits," *IEEE Antennas Wirel. Propag. Lett.*, vol. 13, pp. 209–212, 2014, doi: 10.1109/LAWP.2014.2301277.

[2] J. O. Fiering, P. Hultman, W. Lee, E. D. Light, and S. W. Smith, "High-density flexible interconnect for two-dimensional ultrasound arrays," *IEEE Trans. Ultrason. Ferroelectr. Freq. Control*, vol. 47, no. 3, pp. 764–770, May 2000, doi: 10.1109/58.842067.

[3] S. D. Lubner, S. Kaur, Y. Fu, V. Battaglia, and R. S. Prasher, "Identification and characterization of the dominant thermal resistance in lithium-ion batteries using operando 3-omega sensors," *J. Appl. Phys.*, vol. 127, no. 10, p. 105104, Mar. 2020, doi: 10.1063/1.5134459.

[4] Q. Wang, P. Ping, X. Zhao, G. Chu, J. Sun, and C. Chen, "Thermal runaway caused fire and explosion of lithium ion battery," *J. Power Sources*, vol. 208, pp. 210–224, Jun. 2012, doi: 10.1016/j.jpowsour.2012.02.038.

[5] S. LeBlanc, "Thermoelectric generators: Linking material properties and systems engineering for waste heat recovery applications," *Sustain. Mater. Technol.*, vol. 1–2, pp. 26–35, Dec. 2014, doi: 10.1016/j.susmat.2014.11.002.

ACCEPTED MANUSCRIPT
Review of Scientific Instruments
AIP Publishing
This is the author's peer reviewed, accepted manuscript. However, the online version of record will be different from this version once it has been copyedited and typeset.
PLEASE CITE THIS ARTICLE AS DOI:10.1063/5.0012404

[6] M. C. Rajagopal *et al.*, “Materials-to-device design of hybrid metal-polymer heat exchanger tubes for low temperature waste heat recovery,” *Int. J. Heat Mass Transf.*, vol. 143, p. 118497, Nov. 2019, doi: 10.1016/j.ijheatmasstransfer.2019.118497.
[7] S. Wang, T. Xie, and H. Xie, “Experimental study of the effects of the thermal contact resistance on the performance of thermoelectric generator,” *Appl. Therm. Eng.*, vol. 130, pp. 847–853, Feb. 2018, doi: 10.1016/j.applthermaleng.2017.11.036.
[8] C. V. Madhusudana, *Thermal contact conductance*. Springer, 1996.
[9] H. A. Roddiger and T. D. Mosby, “Interstitial Materials for Low Thermal Resistance Joints in Avionic Equipment,” *SAE Trans.*, vol. 98, pp. 402–412, 1989.
[10] P. K. Schelling, L. Shi, and K. E. Goodson, “Managing heat for electronics,” *Mater. Today*, vol. 8, no. 6, pp. 30–35, Jun. 2005, doi: 10.1016/S1369-7021(05)70935-4.
[11] Y. B. Li, X. M. Lai, and G. L. Chen, “The Influence of Interfacial Thermal Contact Conductance on Resistance Spot Weld Nugget Formation,” *Advanced Materials Research*, 2010. /AMR.97-101.3239 (accessed Apr. 23, 2020).
[12] J. Hu, L. Yang, and M. Whan Shin, “Mechanism and thermal effect of delamination in light-emitting diode packages,” *Microelectron. J.*, vol. 38, no. 2, pp. 157–163, Feb. 2007, doi: 10.1016/j.mejo.2006.08.001.
[13] A. Gaitonde, A. Nimmagadda, and A. Marconnet, “Measurement of interfacial thermal conductance in Lithium ion batteries,” *J. Power Sources*, vol. 343, pp. 431–436, Mar. 2017, doi: 10.1016/j.jpowsour.2017.01.019.
[14] Y. Sungtaek Ju and U. Ghoshal, “Study of interface effects in thermoelectric microrefrigerators,” *J. Appl. Phys.*, vol. 88, no. 7, pp. 4135–4139, Sep. 2000, doi: 10.1063/1.1289776.
[15] A. M. Pettes, M. S. Hodes, and K. E. Goodson, “Optimized Thermoelectric Refrigeration in the Presence of Thermal Boundary Resistance,” *IEEE Trans. Adv. Packag.*, vol. 32, no. 2, pp. 423–430, May 2009, doi: 10.1109/TADVP.2008.924221.
[16] R. Prasher, “Thermal Interface Materials: Historical Perspective, Status, and Future Directions,” *Proc. IEEE*, vol. 94, no. 8, pp. 1571–1586, Aug. 2006, doi: 10.1109/JPROC.2006.879796.
[17] K. Lo, Wenjun Liu, L. Pileggi, and Mehdi Asheghi, “An electronic packaging design for reduction of thermal interface resistance,” in *Thermal and Thermomechanical Proceedings 10th Intersociety Conference on Phenomena in Electronics Systems, 2006. ITHERM 2006.*, May 2006, p. 4 pp. – 528, doi: 10.1109/ITHERM.2006.1645389.
[18] A. Vassighi and M. Sachdev, “Thermal runaway in integrated circuits,” *IEEE Trans. Device Mater. Reliab.*, vol. 6, no. 2, pp. 300–305, Jun. 2006, doi: 10.1109/TDMR.2006.876577.
[19] A. L. Moore and L. Shi, “Emerging challenges and materials for thermal management of electronics,” *Mater. Today*, vol. 17, no. 4, pp. 163–174, May 2014, doi: 10.1016/j.mattod.2014.04.003.
[20] P. Kapitza, “The study of heat transfer in helium II,” *J PhysMoscow*, vol. 4, p. 181, 1941.
[21] H.-C. Chien, D.-J. Yao, M.-J. Huang, and T.-Y. Chang, “Thermal conductivity measurement and interface thermal resistance estimation using SiO2 thin film,” *Rev. Sci. Instrum.*, vol. 79, no. 5, p. 054902, May 2008, doi: 10.1063/1.2927253.
[22] D.-W. Oh, S. Kim, J. A. Rogers, D. G. Cahill, and S. Sinha, “Interfacial Thermal Conductance of Transfer-Printed Metal Films,” *Adv. Mater.*, vol. 23, no. 43, pp. 5028–5033, 2011, doi: 10.1002/adma.201102994.
[23] D. G. Cahill, “Thermal conductivity measurement from 30 to 750 K: the 3ω method,” *Rev. Sci. Instrum.*, vol. 61, no. 2, pp. 802–808, Feb. 1990, doi: 10.1063/1.1141498.
[24] T. Borca-Tasciuc, A. R. Kumar, and G. Chen, “Data reduction in 3ω method for thin-film thermal conductivity determination,” *Rev. Sci. Instrum.*, vol. 72, no. 4, pp. 2139–2147, Mar. 2001, doi: 10.1063/1.1353189.
[25] T. Yamane, N. Nagai, S. Katayama, and M. Todoki, “Measurement of thermal conductivity of silicon dioxide thin films using a 3ω method,” *J. Appl. Phys.*, vol. 91, no. 12, pp. 9772–9776, May 2002, doi: 10.1063/1.1481958.

Review of Scientific Instruments
ACCEPTED MANUSCRIPT
This is the author's peer reviewed, accepted manuscript. However, the online version of record will be different from this version once it has been copyedited and typeset.
PLEASE CITE THIS ARTICLE AS DOI:10.1063/5.0012404
AIP Publishing

1 [26] M. G. Burzo, P. L. Komarov, and P. E. Raad, “Thermal transport properties of gold-covered thin-
2 film silicon dioxide,” *IEEE Trans. Compon. Packag. Technol.*, vol. 26, no. 1, pp. 80–88, Mar. 2003,
3 doi: 10.1109/TCAPT.2003.811467.
4 [27] D. G. Cahill, “Analysis of heat flow in layered structures for time-domain thermoreflectance,” *Rev.*
5 *Sci. Instrum.*, vol. 75, no. 12, pp. 5119–5122, Nov. 2004, doi: 10.1063/1.1819431.
6 [28] A. J. Schmidt, R. Cheaito, and M. Chiesa, “A frequency-domain thermoreflectance method for the
7 characterization of thermal properties,” *Rev. Sci. Instrum.*, vol. 80, no. 9, p. 094901, Sep. 2009, doi:
8 10.1063/1.3212673.
9 [29] J. Zhu, D. Tang, W. Wang, J. Liu, and R. Yang, “Frequency-Domain Thermoreflectance Technique
10 for Measuring Thermal Conductivity and Interface Thermal Conductance of Thin Films,” Mar.
11 2011, pp. 371–379, doi: 10.1115/IHTC14-22522.
12 [30] M. Rohde *et al.*, “Intercomparison of thermal diffusivity measurements on CuCrZr and PMMA,”
13 *High Temp High Press*, vol. 42, pp. 469–474, 2013.
14 [31] R. Garrelts, A. Marconnet, and X. Xu, “Assessment of Thermal Properties via Nanosecond
15 Thermoreflectance Method,” *Nanoscale Microscale Thermophys. Eng.*, vol. 19, no. 4, pp. 245–257,
16 Oct. 2015, doi: 10.1080/15567265.2015.1078425.
17 [32] C. Yuan, W. M. Waller, and M. Kuball, “Nanosecond transient thermoreflectance method for
18 characterizing anisotropic thermal conductivity,” *Rev. Sci. Instrum.*, vol. 90, no. 11, p. 114903, Nov.
19 2019, doi: 10.1063/1.5099961.
20 [33] V. Singhal, P. J. Litke, A. F. Black, and S. V. Garimella, “An experimentally validated thermo-
21 mechanical model for the prediction of thermal contact conductance,” *Int. J. Heat Mass Transf.*, vol.
22 48, no. 25, pp. 5446–5459, Dec. 2005, doi: 10.1016/j.ijheatmasstransfer.2005.06.028.
23 [34] R. Kempers, P. Kolodner, A. Lyons, and A. J. Robinson, “A high-precision apparatus for the
24 characterization of thermal interface materials,” *Rev. Sci. Instrum.*, vol. 80, no. 9, p. 095111, Sep.
25 2009, doi: 10.1063/1.3193715.
26 [35] N. N. Verma and S. Mazumder, “Extraction of thermal contact conductance of metal–metal contacts
27 from scale-resolved direct numerical simulation,” *Int. J. Heat Mass Transf.*, vol. 94, pp. 164–173,
28 Mar. 2016, doi: 10.1016/j.ijheatmasstransfer.2015.11.026.
29 [36] J. J. Fuller and E. E. Marotta, “Thermal contact conductance of metal/polymer joints: an analytical
30 and experimental investigation,” *J. Thermophys. Heat Transf.*, vol. 15, no. 2, pp. 228–238, 2001.
31 [37] R. S. Prasher and J. C. Matayabas, “Thermal contact resistance of cured gel polymeric thermal
32 interface material,” *IEEE Trans. Compon. Packag. Technol.*, vol. 27, no. 4, pp. 702–709, Dec. 2004,
33 doi: 10.1109/TCAPT.2004.838883.
34 [38] M. Grujicic, C. L. Zhao, and E. C. Dusel, “The effect of thermal contact resistance on heat
35 management in the electronic packaging,” *Appl. Surf. Sci.*, vol. 246, no. 1, pp. 290–302, Jun. 2005,
36 doi: 10.1016/j.apsusc.2004.11.030.
37 [39] K. V. Valavala, K. D. Coulson, M. C. Rajagopal, D. Gelda, and S. Sinha, “Chapter 4 - Thermal
38 Engineering at the Limits of the CMOS Era,” in *Handbook of Thin Film Deposition (Fourth*
39 *Edition)*, William Andrew Publishing, 2018, pp. 63–101.
40 [40] “DuPont Pyralux LF Laminates.” [Online]. Available:
41 https://www.dupont.com/content/dam/dupont/amer/us/en/products/ei-
42 transformation/documents/PyraluxLFclad_DataSheet.pdf.
43 [41] M. A. Uddin, M. O. Alam, Y. C. Chan, and H. P. Chan, “Adhesion strength and contact resistance
44 of flip chip on flex packages—effect of curing degree of anisotropic conductive film,”
45 *Microelectron. Reliab.*, vol. 44, no. 3, pp. 505–514, Mar. 2004, doi: 10.1016/S0026-2714(03)00185-
46 9.
47 [42] E. Mariani and E. Ghassemieh, “Microstructure evolution of 6061 O Al alloy during ultrasonic
48 consolidation: An insight from electron backscatter diffraction,” *Acta Mater.*, vol. 58, no. 7, pp.
49 2492–2503, Apr. 2010, doi: 10.1016/j.actamat.2009.12.035.

Review of Scientific Instruments ACCEPTED MANUSCRIPT
This is the author's peer reviewed, accepted manuscript. However, the online version of record will be different from this version once it has been copyedited and typeset.
PLEASE CITE THIS ARTICLE AS DOI:10.1063/5.0012404
AIP Publishing

[43] A. K. Pandey, K. C. Nayak, and S. S. Mahapatra, "Characterization of friction stir spot welding between copper and poly-methyl-methacrylate (PMMA) sheet," *Mater. Today Commun.*, vol. 19, pp. 131–139, Jun. 2019, doi: 10.1016/j.mtcomm.2019.01.010.

[44] K. Kurabayashi, M. Asheghi, M. Touzelbaev, and K. E. Goodson, "Measurement of the thermal conductivity anisotropy in polyimide films," *J. Microelectromechanical Syst.*, vol. 8, no. 2, pp. 180–191, Jun. 1999, doi: 10.1109/84.767114.

[45] Y.-S. Lin and H.-M. Liu, "Enhanced adhesion of plasma-sputtered copper films on polyimide substrates by oxygen glow discharge for microelectronics," *Thin Solid Films*, vol. 516, no. 8, pp. 1773–1780, Feb. 2008, doi: 10.1016/j.tsf.2007.07.162.

[46] K. K. Chakravorty, C. P. Chien, J. M. Cech, M. H. Tanielian, and P. L. Young, "High-density interconnection using photosensitive polyimide and electroplated copper conductor lines," *IEEE Trans. Compon. Hybrids Manuf. Technol.*, vol. 13, no. 1, pp. 200–206, Mar. 1990, doi: 10.1109/33.52871.

[47] H. L. Gower, R. R. G. M. Pieters, and I. M. Richardson, "Pulsed laser welding of metal-polymer sandwich materials using pulse shaping," *J. Laser Appl.*, vol. 18, no. 1, pp. 35–41, Feb. 2006, doi: 10.2351/1.2080307.

[48] Y. Meng *et al.*, "Ultrasonic Welding of Soft Polymer and Metal: A Preliminary Study," presented at the ASME 2019 14th International Manufacturing Science and Engineering Conference, Nov. 2019, doi: 10.1115/MSEC2019-2938.

[49] F. C. Krebs, "Roll-to-roll fabrication of monolithic large-area polymer solar cells free from indium-tin-oxide," *Sol. Energy Mater. Sol. Cells*, vol. 93, no. 9, pp. 1636–1641, Sep. 2009, doi: 10.1016/j.solmat.2009.04.020.

[50] T.-S. Kim *et al.*, "All-solution-processed ITO-free polymer solar cells fabricated on copper sheets," *Sol. Energy Mater. Sol. Cells*, vol. 98, pp. 168–171, Mar. 2012, doi: 10.1016/j.solmat.2011.09.058.

[51] S. J. Tomczak *et al.*, "Space Survivability of Main-Chain and Side-Chain POSS-Kapton Polyimides," *AIP Conf. Proc.*, vol. 1087, no. 1, pp. 505–518, Jan. 2009, doi: 10.1063/1.3076863.

[52] "DuPont Kapton properties." [Online]. Available: http://www.dupont.com/content/dam/dupont/products-and-services/membranes-and-films/polyimde-films/documents/DEC-Kapton-summary-of-properties.pdf.

[53] J. Han, Z. Tan, K. Sato, and M. Shikida, "Three-dimensional interconnect technology on a flexible polyimide film," *J. Micromechanics Microengineering*, vol. 14, no. 1, pp. 38–48, Aug. 2003, doi: 10.1088/0960-1317/14/1/306.

[54] J. H. Brannon, J. R. Lankard, A. I. Baise, F. Burns, and J. Kaufman, "Excimer laser etching of polyimide," *J. Appl. Phys.*, vol. 58, no. 5, pp. 2036–2043, Sep. 1985, doi: 10.1063/1.336012.

[55] M. C. Rajagopal, K. V. Valavala, D. Gelda, J. Ma, and S. Sinha, "Fabrication and characterization of thermocouple probe for use in intracellular thermometry," *Sens. Actuators Phys.*, vol. 272, pp. 253–258, Apr. 2018, doi: 10.1016/j.sna.2018.02.004.

[56] G. Kuntumalla *et al.*, "Joining Techniques for Novel Metal Polymer Hybrid Heat Exchangers," presented at the ASME 2019 International Mechanical Engineering Congress and Exposition, Jan. 2020, doi: 10.1115/IMECE2019-10621.

[57] J. Dellinger, "The temperature coefficient of resistance of copper," *J. Frankl. Inst.*, vol. 170, no. 3, pp. 213–216, 1910.

[58] A. von Glasow, A. H. Fischer, and G. Steinlesberger, "Using the temperature coefficient of the resistance (TCR) as early reliability indicator for stressvoiding risks in Cu interconnects," in *2003 IEEE International Reliability Physics Symposium Proceedings, 2003. 41st Annual.*, Mar. 2003, pp. 126–131, doi: 10.1109/RELPHY.2003.1197732.

[59] M. Daal, N. Zobrist, N. Kellaris, B. Sadoulet, and M. Robertson, "Properties of selected structural and flat flexible cabling materials for low temperature applications," *Cryogenics*, vol. 98, pp. 47–59, Mar. 2019, doi: 10.1016/j.cryogenics.2018.10.019.

[60] K. Alzoubi, S. Lu, B. Sammakia, and M. Poliks, "Experimental and Analytical Studies on the High Cycle Fatigue of Thin Film Metal on PET Substrate for Flexible Electronics Applications," *IEEE*

ACCEPTED MANUSCRIPT
Review of Scientific Instruments
AIP Publishing
This is the author's peer reviewed, accepted manuscript. However, the online version of record will be different from this version once it has been copyedited and typeset.
PLEASE CITE THIS ARTICLE AS DOI: 10.1063/5.0012404

1 *Trans. Compon. Packag. Manuf. Technol.*, vol. 1, no. 1, pp. 43–51, Jan. 2011, doi:
2 10.1109/TCPMT.2010.2100911.
3 [61] P. Kah, R. Suoranta, J. Martikainen, and C. Magnus, "TECHNIQUES FOR JOINING
4 DISSIMILAR MATERIALS: METALS AND POLYMERS.," *Rev. Adv. Mater. Sci.*, vol. 36, no. 2,
5 2014.
6 [62] K. C. Otiaba, N. N. Ekere, R. S. Bhatti, S. Mallik, M. O. Alam, and E. H. Amalu, "Thermal
7 interface materials for automotive electronic control unit: Trends, technology and R&D challenges,"
8 *Microelectron. Reliab.*, vol. 51, no. 12, pp. 2031–2043, Dec. 2011, doi:
9 10.1016/j.microrel.2011.05.001.
10 [63] K. Coulson, S. Sinha, and N. Miljkovic, "Analysis of modular composite heat pipes," *Int. J. Heat*
11 *Mass Transf.*, vol. 127, pp. 1198–1207, Dec. 2018, doi: 10.1016/j.ijheatmasstransfer.2018.07.140.
12 [64] R. G. Schmidt and J. P. Bell, "Epoxy adhesion to metals," in *Epoxy Resins and Composites II*,
13 Berlin, Heidelberg, 1986, pp. 33–71, doi: 10.1007/BFb0017914.

a

w

Cu

Heater, T_h

25 μm

Adhesive

25 μm

Kapton

t_p

Adhesive

25 μm

Cu

Sensor, T_s

25 μm

Sink

Q_{DC}

T_h

R''_{mp}

R''_{p}

R''_{mp}

R''_{Cu}

R''_{∞}

T_{∞}

b

$I_{AC(h)} + I_{DC}$

$V_{AC(h)}$

$I_{AC(s)}$

$V_{AC(s)}$

a

Error, $\left|\frac{\Delta R''_{mp}}{R''_{mp}}\right|$

1

0.1

0.01

0.001

b

75 μm

50 μm

t_p=25 μm

c

10^{-5} 10^{-4} 10^{-3}

Width, w (m)

b Error ~113.1%

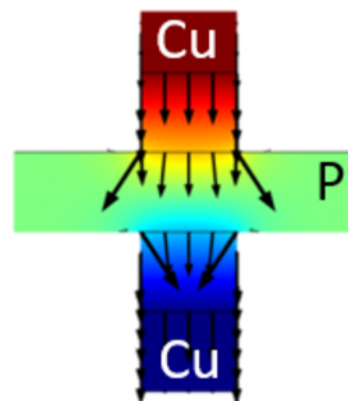

c Error ~1.8%

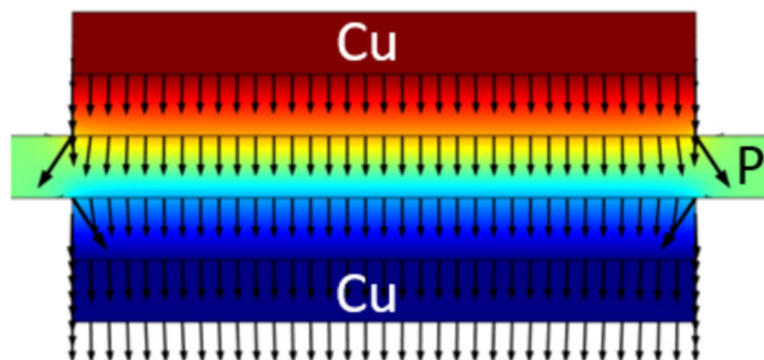

a

Error, $\left|\frac{\Delta R''_{mp}}{R''_{mp}}\right|$

75 μm

50 μm

t_p = 25 μm

b

c

R''_{mp}(m^2 KW^{-1})

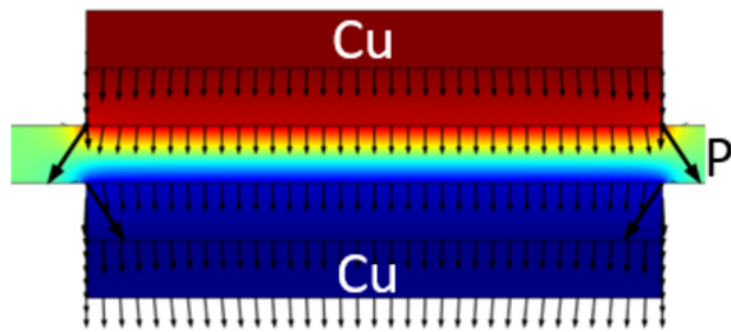

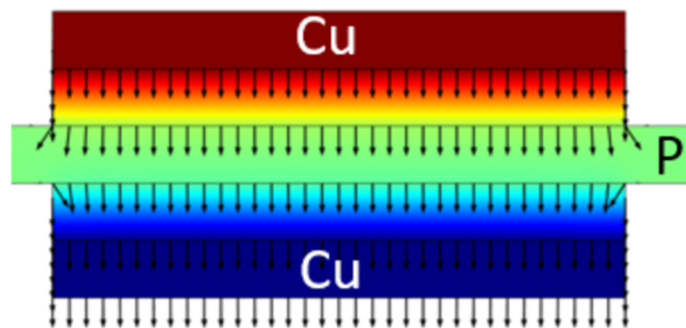

a

10^{-3} m^2KW^{-1}

10^{-4}

10^{-5}

0.5 K

ΔT limited

ΔT_h-ΔT_s (K)

100
10
1
0.1
0.01

10^{-5} 10^{-4} 10^{-3}

Width, w (m)

b

w=250 μm

I_{DC} limited

1.0 A

I_{DC} (A)

2.0
1.5
1.0
0.5
0.0

10^{-5} 10^{-4} 10^{-3}

Width, w (m)

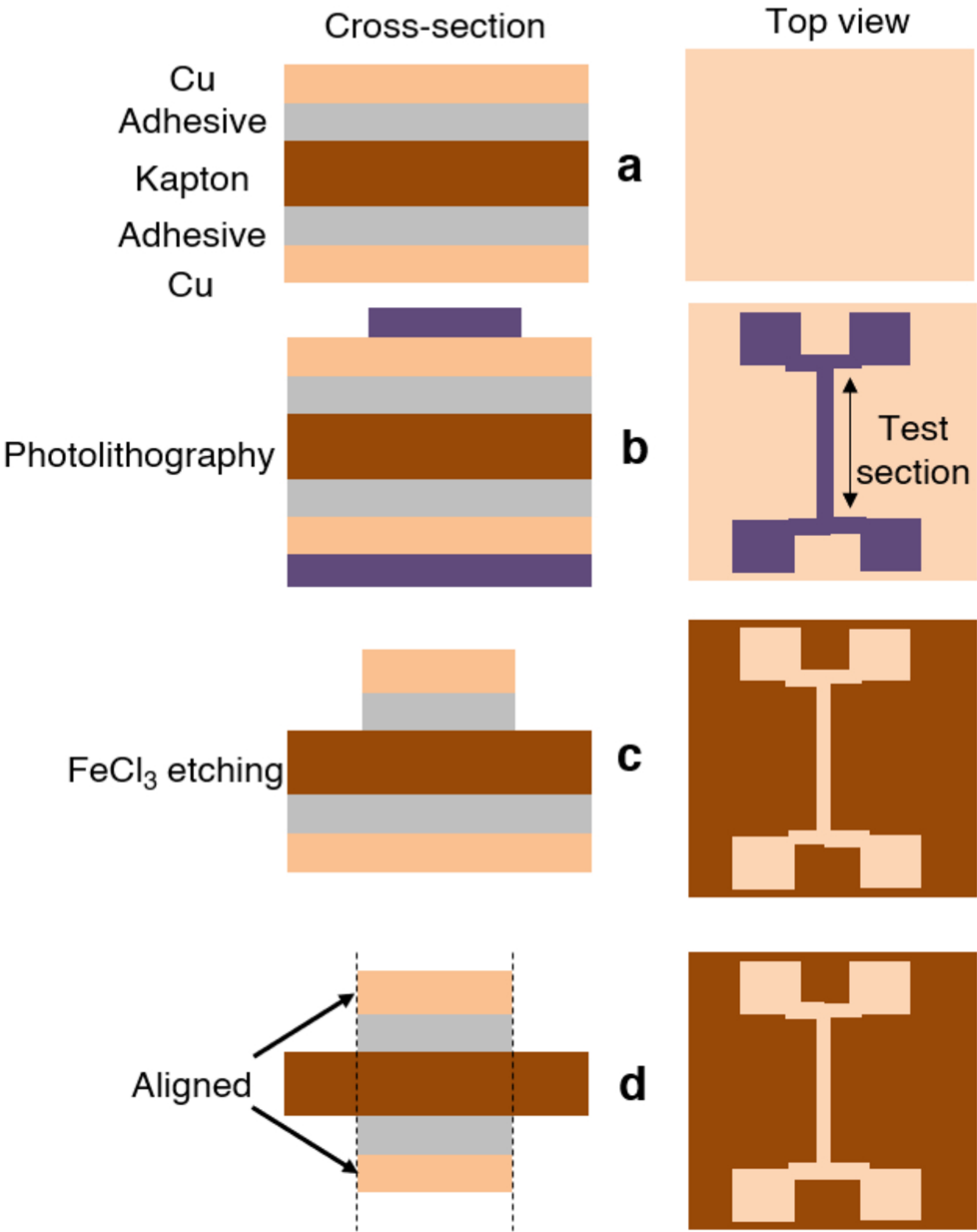

Cross-section
Top view
Cu
Adhesive
Kapton
Adhesive
Cu
a
Photolithography
b
Test section
FeCl3 etching
c
Aligned
d

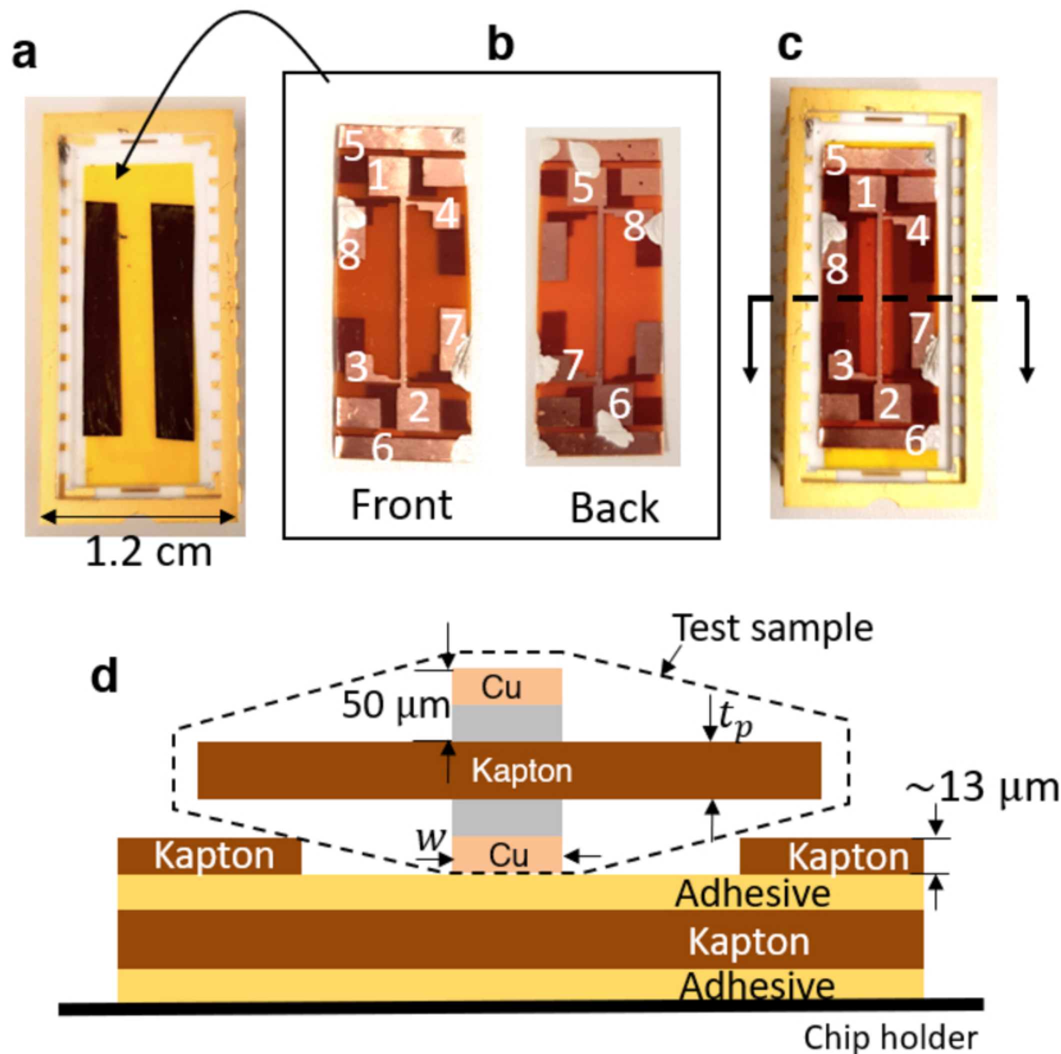
a
b
c
Front
Back
1.2 cm
5
1
4
8
7
3
2
6
d
Test sample
Cu
50 μm
t_p
Kapton
~13 μm
w
Kapton
Cu
Kapton
Adhesive
Kapton
Adhesive
Chip holder

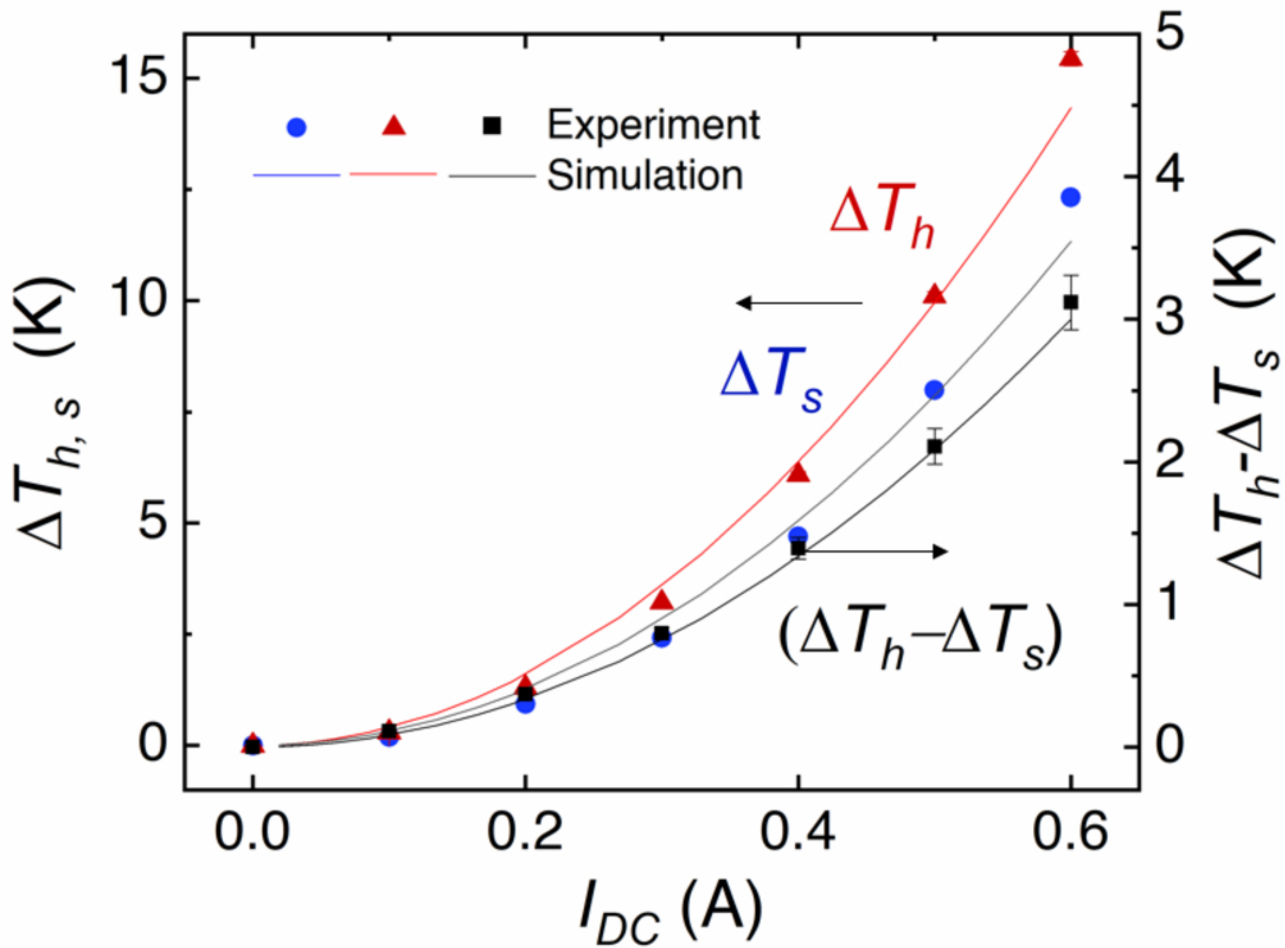

Experiment
Simulation
ΔT_h
ΔT_s
$(\Delta T_h - \Delta T_s)$
$\Delta T_{h,s}$ (K)
ΔT_h-ΔT_s (K)
I_{DC} (A)
0.0
0.2
0.4
0.6
0
5
10
15
1
2
3
4

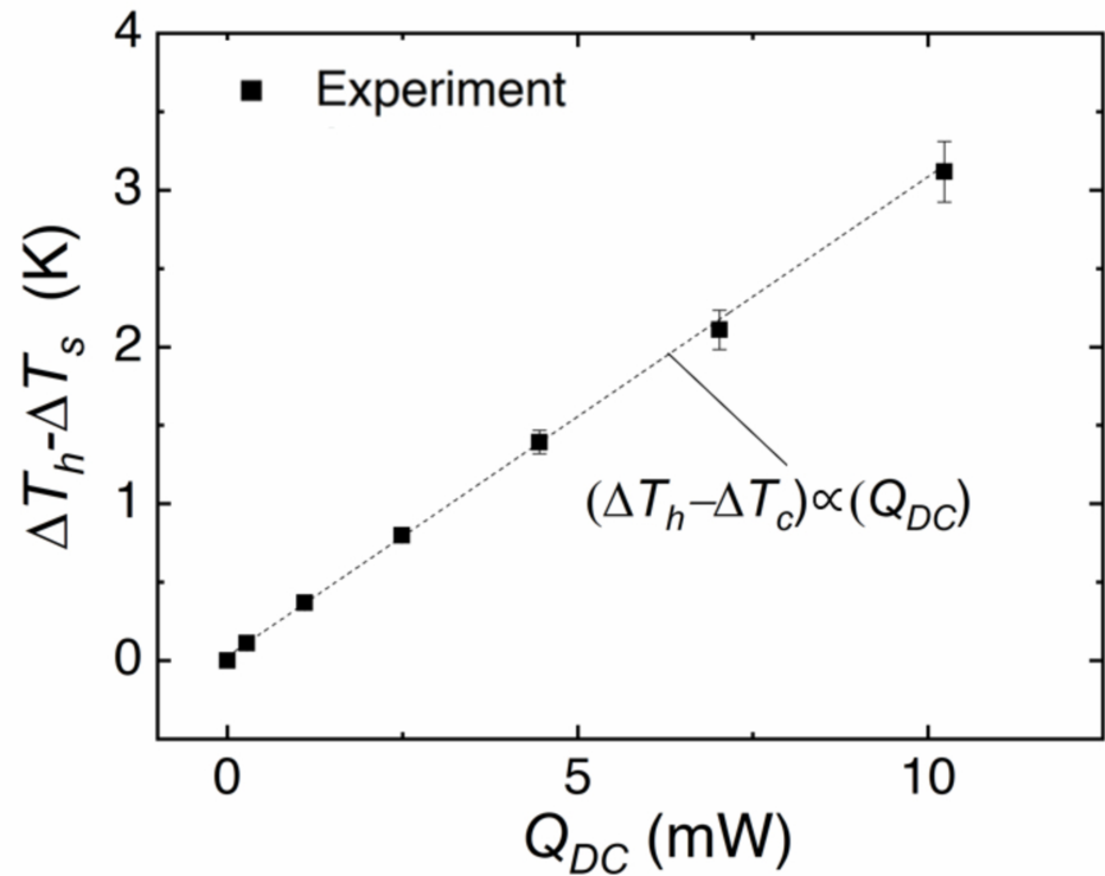

Experiment
$(\Delta T_h - \Delta T_c) \propto (Q_{DC})$
ΔT_h-ΔT_s (K)
Q_{DC} (mW)
0
1
2
3
4
0
5
10

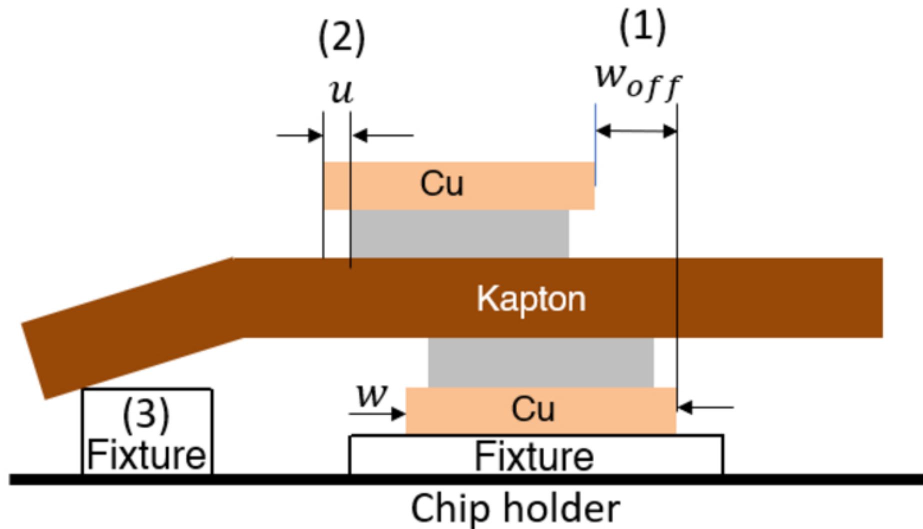

(2)
u
(1)
w_{off}
Cu
Kapton
w
Cu
(3)
Fixture
Fixture
Chip holder

a

t_p= 25 μm
10^{-5} m^2KW^{-1}

c

t_p= 100 μm
10^{-4} m^2KW^{-1}

ΔT_{comp} (K)

2
1
0
-1
-2

0.0 0.1 0.2 0.3 0.4

Q_{ref}/Q_{DC}